ACS APPLIED POLYMER MATERIALS

pubs.acs.org/acsapm Article

Corrosion Protective Coatings from Poly(heterocyclic diphenylamine): Polyaniline Analogues

Raymond Femi Awoyemi, Mohammed Almtiri, Hari Giri, Colleen N. Scott, and David O. Wipf*

Cite This: *ACS Appl. Polym. Mater.* 2024, 6, 3060−3072 Read Online

ACCESS | Metrics & More | Article Recommendations | Supporting Information

ABSTRACT: This study explores conducting polymers with side chains containing long, branched alkyl groups as candidates for corrosion suppression coatings. These polymers, containing carbazole, phenothiazine, and phenoxazine cores, may be considered as analogues to polyaniline, which is often employed in corrosion control applications. The polymers are prepared from the corresponding dibrominated carbazole, phenothiazine, and phenoxazine monomers with 2,5-dimethyl-1,4-phenylenediamine by the Buchwald−Hartwig coupling reaction. The effectiveness of these coatings for corrosion suppression was tested by potentiodynamic polarization studies and electrochemical impedance spectroscopy. The morphology of the coatings was characterized by scanning electron microscopy (SEM) and atomic force microscopy (AFM). Corrosion testing of coated AISI 4130 steels in 3.5 wt % NaCl showed that the phenothiazine- and carbazole-containing polymers display excellent corrosion resistance. The protection efficiency (PE) of 95.9% for phenothiazine outperformed the other polymers, including polyaniline coating. SEM images indicate that the polymers are still uniformly coated with stable morphology after 24 h of exposure to corrosive media. These results suggest that phenothiazine- and carbazole-based PANI analogues may be candidates for protective organic coatings in transportation, aviation, marine, and oil and gas industrial applications.

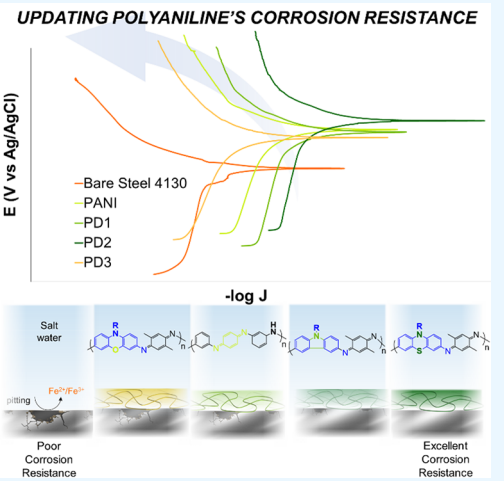

KEYWORDS: *corrosion, polyaniline, polyaniline analogues, poly(heterocyclic diphenylamine), phenothiazine, carbazole, phenoxazine, conducting polymer*

1. INTRODUCTION

The ability of conducting polymers (CPs) to impart corrosion resistance to some metals has attracted researchers for many years.[1,2] Conducting polymers such as polypyrrole (PPy), polythiophene (PTh), poly(3,4-ethylenedioxythiophene) (PEDOT), polyaniline (PANI), poly(*p*-phenylene) (PPP), poly(*p*-phenylenevinylene) (PPV), and polycarbazole (PCz) have all been proposed as components of corrosion protection coatings.[2−6] PANI is one of the most studied conducting polymers to date due to its exceptional environmental stability in the doped state, good mechanical properties, and high electrical conductivity.[1,6−8] Since DeBerry reported using PANI as a protective coating for stainless steels, PANI-based coatings have been used to improve the corrosion protection of many metals, including aluminum, titanium, magnesium, aluminum alloys, steel, copper, and zinc.[5,9−15] The redox activity of PANI is implicated in providing anodic corrosion protection because it shifts the equilibrium potential of the coated substrate in a positive (i.e., anodic) direction.[6,12,16,17] PANI exists in three interconvertible forms depending on the redox state: the partially oxidized emeraldine base (EB), fully oxidized pernigraniline base (PB), and fully reduced leucoemeraldine base (LB) form. All of these forms of PANI are insulators. Moreover, PANI has been used as an anticorrosion coating in diverse corrosive media. The EB form is the most common structure of PANI due to its high chemical stability and is widely employed as anticorrosion coating for ferrous and non-ferrous metals and alloys.[4,5] The EB form, for instance, is very effective in combating corrosion from NaCl.[4,5] EB is converted to conducting emeraldine salt (ES) by acid doping, which leads to effective corrosion control in acidic solutions.[18,19] PANI's protective coating for metallic surfaces provides high corrosion resistance[14] by forming adjacent layers of passive metallic oxide such as Fe_3O_4, α-Fe_2O_3, and γ-Fe_2O_3[2,6,20,21] or forming nitrides[22] and by promoting the passivation of the coated substrates. The metal surface is shielded from further corrosion by these thick oxide layers that serve as physical barrier

Received: October 1, 2023
Revised: January 28, 2024
Accepted: February 28, 2024
Published: March 11, 2024

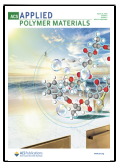

https://doi.org/10.1021/acsapm.3c02347
ACS Appl. Polym. Mater. 2024, 6, 3060−3072

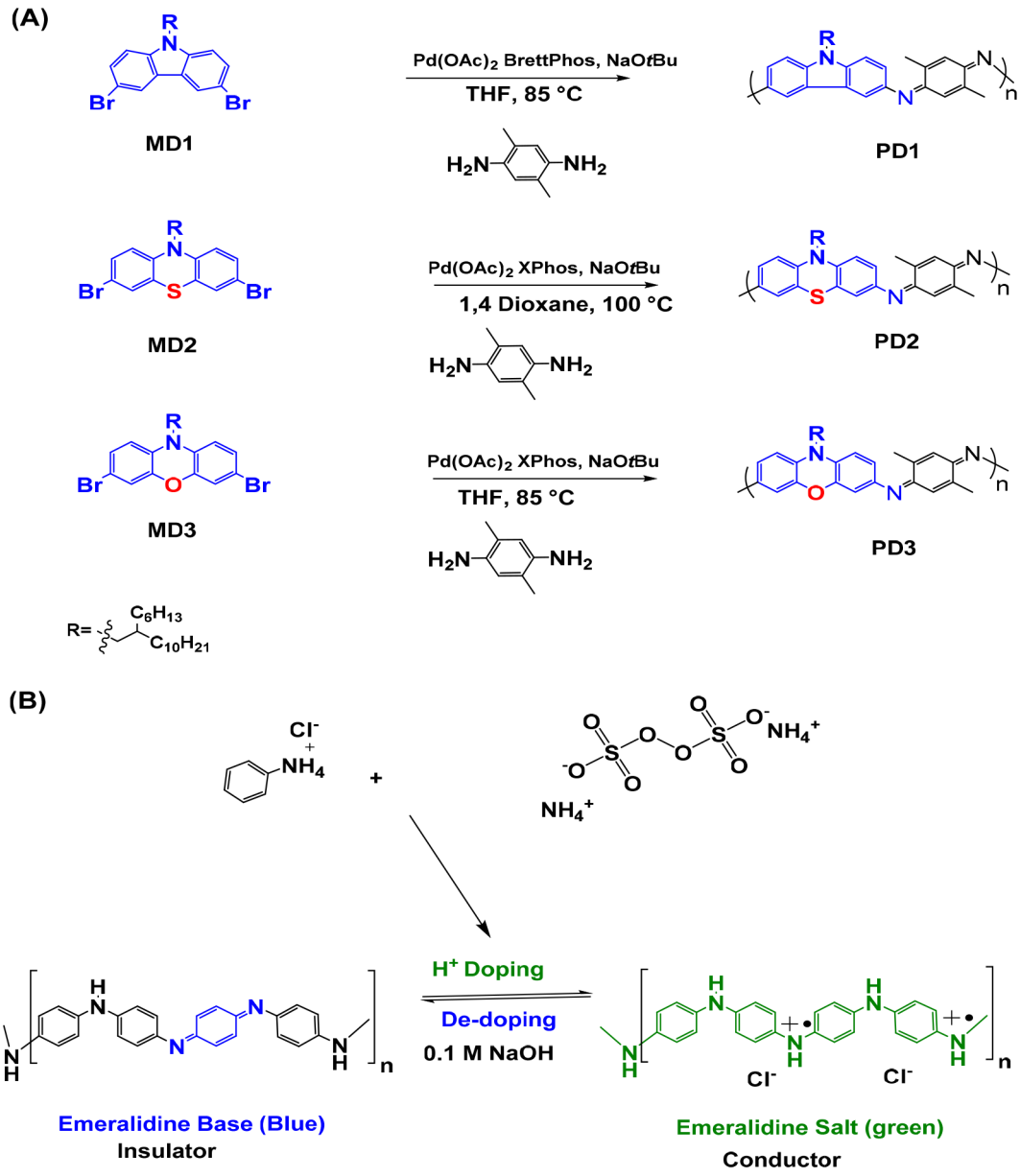

Figure 1. (A) Synthetic route of PANI analogues. (B) Synthetic route to PANI nanofibers from aniline hydrochloride.

protection.[2,5,6] The effectiveness of barrier protection can be increased by enhancing PANI coating's bonding (adhesion) abilities to the metal−polymer interface.[2,6,17,20]

Despite its wide use for corrosion protection, PANI has limitations as a material. One of these limitations is the reported poor adhesion of PANI to metal surfaces.[3,23,24] The poor solubility of PANI in most organic solvents limits its processability for industrial applications.[6,25] Consequently, electrochemical oxidative polymerization of aniline may be used to form PANI films on metals and alloys.[2,6] Developing conducting polymers with improved electrochemical and mechanical stability compared to PANI is needed to improve coating application from organic solvents.[26,27] Methods such as the modification of monomer structure, use of soluble precursors, and formation of copolymers or composites have been introduced to improve PANI's properties (conductivity, solubility, etc.).[3,15,23,24,28−34] Our efforts are to incorporate large, branched alkyl chains into the polymer and replace the aniline backbone with precursors (carbazole, phenothiazine, and phenoxazine) that can improve solubility (e.g., by derivatization with alkyl or other solubilizing groups) in common organic solvents, thereby enhancing their processability for wide organic coating application, explicitly investigating their anticorrosion properties with a view of projecting these materials as promising candidates for corrosion control coatings.

In this paper, we demonstrate the synthesis of processable PANI analogues incorporating long branched alkyl chains by the copolymerization of 2,5-dimethyl-*p*-phenylenediamine (PPDA) with 3,6-dibromo-9-(2-hexyldecyl)carbazole, 3,7-dibromo-10-(2-hexyldecyl)phenothiazine, and 3,7-dibromo-10-(2-hexyldecyl)phenoxazine by the Buchwald/Hartwig reaction for anticorrosion coatings. Specifically, the polymers are poly(10-(2-hexyldecyl)carbazole-3,7-diyl-*alt*-2,5-dimethyl-*p*-phenylenediamine) (**PD1**), poly(10-(2-hexyldecyl)-phenothiazine-3,7-diyl-*alt*-2,5-dimethyl-*p*-phenylenediamine) (**PD2**), and poly(10-(2-hexyldecyl)phenoxazine-3,7-diyl-*alt*-

https://doi.org/10.1021/acsapm.3c02347
ACS Appl. Polym. Mater. 2024, 6, 3060−3072

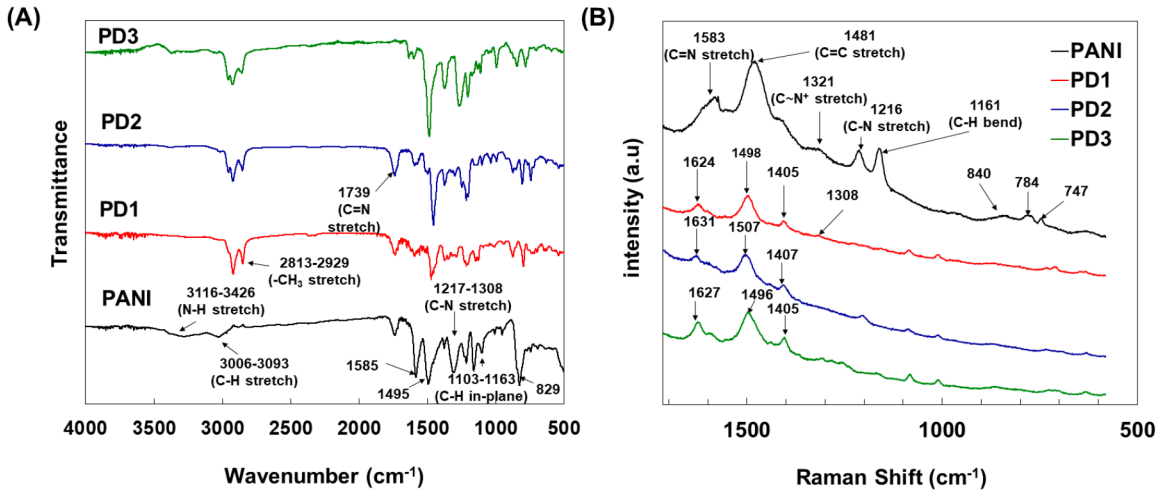

Figure 2. (A) ATR-IR spectra of PANI, **PD1**, **PD2**, and **PD3**. (B) Raman spectra of PANI, **PD1**, **PD2**, and **PD3**.

2,5-dimethyl-*p*-phenylenediamine) (**PD3**). The polymers were successfully characterized by ATR-IR, UV, and ^{1}H NMR spectroscopy, and solution was deposited from various common organic solvents. These polymers were then examined as corrosion-protective barrier coatings and compared to PANI coatings, as the EB form for both PANI analogues and PANI was used in this study. Corrosion resistance efficiency is tested for the films on steel in 3.5 wt % NaCl solution using potentiodynamic polarization and electrochemical impedance spectroscopy (EIS). Superior corrosion inhibition by the phenothiazine-core coating on steel in comparison to PANI was demonstrated in this work, introducing it as an option for corrosion control applications. To our knowledge, this work is the first report on these PANI analogues for use as in corrosion protection.

2. EXPERIMENTAL SECTION

2.1. Materials. All chemicals used in this study were reagent grade and used without further purification unless otherwise stated. A solvent purification system was used to obtain dry, degassed tetrahydrofuran (THF), dichloromethane (DCM), and toluene. Aniline hydrochloride and ammonium persulfate (APS, 99%) were purchased from Fisher Scientific (Princeton, NJ), and acetone (HPLC grade), *N*-methyl-2-pyrrolidone (NMP), and *N*,*N*-dimethylformamide (DMF) (ACS reagent grade, 99.8%) were purchased from Sigma-Aldrich Chemicals (USA). Deionized water with resistivity of not less than 18.0 MΩ cm was used throughout the analysis.

2.2. Substrate Preparation. Chromium−molybdenum alloy steel (AISI 4130AQ) coupons of dimensions 5.08 cm × 5.08 cm × 0.16 cm were obtained from OnlineMetals.com. The steel is specified as 6345ASTM A505/506 normalized or otherwise heat-treated with the following reported composition (wt %) of 0.32 C, 0.46 Mn, 0.008 P, 0.001 S, 0.19 Si, 0.039 Al, 0.03 Cu, 0.02 Ni, 0.91 Cr, 0.15 Mo, 0.006 Sn, 0.005 V, 0.001 Nb, 0.0002 B, 0.0040 Ti, 0.0027 Ca, 0.0050 N, and Fe, the balance. The steel coupons were polished using SiC paper in the order of 240, 400, and 800 grit. After polishing, the coupons were sonicated in acetone for 15 min, air-dried, and immediately coated with the polymer.

2.3. Synthesis of Polyaniline Analogues. The monomers 3,6-dibromo-9-(2-hexyldecyl)carbazole (**MD1**), 3,7-dibromo-10-(2-hexyldecyl)phenothiazine (**MD2**), and 3,7-dibromo-10-(2-hexyldecyl)phenoxazine (**MD3**) were prepared using a previously reported method for similar monomers.[27,35] Synthesis of the polymers followed previously reported methods (Figure 1A).[26−28,35] **MD1**, **MD2**, and **MD3** (1 equiv), 2,5-dimethyl-*p*-phenylenediamine (1.05 equiv), NaO*t*Bu (2.8 equiv), Pd(OAc)$_2$ (0.05 equiv), and Brettphos (0.075 equiv for **MD1**)/Xphos (0.075 equiv for **MD2** and **MD3**) were all added into an oven-dried microwave vial containing a magnetic stir bar, which was capped before being removed from the glovebox. For the product desired, either 5 mL of freshly distilled THF or dioxane (5 mL) was added to the mixture, and the vial was placed in an oil bath at 85 or 100 °C and stirred vigorously for 24 h. The reaction mixture was cooled to room temperature and diluted with DCM. The mixture was then filtered through diatomite and the filtrate concentrated under reduced pressure to give the crude polymer. The crude polymer was purified using a Soxhlet extractor with ethanol, acetone, hexane, and finally collected in chloroform. Polymers **PD1**, **PD2**, and **PD3** were concentrated under reduced pressure to give 81%, 70%, and 52% yield, respectively.

2.4. Preparation of PANI. PANI was synthesized by first dissolving aniline hydrochloride (1.3 g, 0.1 mol) in 70 mL of deionized water. This solution was cooled to 0 °C in an ice bath and oxidized with aqueous APS (2.28 g in 30 mL) added dropwise over 20 min with vigorous stirring during the initial oxidation and then with continuous stirring for 24 h. The resulting product was filtered and washed with deionized water until a clear filtrate was observed. The polyaniline was dedoped with 0.1 M sodium hydroxide (NaOH) in a 2-neck flask with vigorous stirring and subsequent stirring for 24 h (Figure 1B). The resulting solid was then filtered and dried under vacuum at 50 °C for 24 h to yield blue needle-shaped crystals.

2.5. Coating Preparation. The polymer coating solution was made by dissolving the polymer in 10 mL of a 1:3 toluene/chloroform mixture at a concentration of 190 mg/mL. About 1 mL of the resulting solution was dropped on the metal test coupon prior to being spin-coated at 300 rpm for 3 min (WS-400 Spin Processor, Laurell Technologies, Lansdale, PA). A PANI coating was prepared by dropping 1 mL of a PANI solution (190 mg/mL in NMP) on the steel substrates prior to spin-coating as described above. The PANI-coated steel was vacuum-dried for 36 h at 95 °C.

2.6. Characterizations and Instrumentation. XRD analyses of the samples (powder) were acquired by a Bruker D8 Advance X-ray diffractometer (Germany) using Cu Kα radiation (30 kV, 20 mA, and λ = 1.54 Å). Data were acquired with 4 s steps of 0.02° in the range of 2θ = 5°−60°. The ratio between the intensity of the crystalline peaks to the sum of the crystalline and amorphous intensities was used in calculating the percentage crystallinity of the samples. A Bruker Dimension Icon atomic force microscope (AFM) using the PeakForce quantitative Nanoscale Mechanical Characterization Mode (QNM) was used to quantify the surface energy of the rough coated surfaces and to measure the adhesion force of the coated steels. The surface morphology of the coated substrates was acquired with a scan area of 5 μm × 5 μm. Field emission SEM (FESEM, JEOL 6500F) images were acquired at 5 kV to measure the surface morphologies of the uncoated and coated substrates. Samples were coated with ≈15 nm Pt for the FESEM/

https://doi.org/10.1021/acsapm.3c02347
ACS Appl. Polym. Mater. 2024, 6, 3060−3072

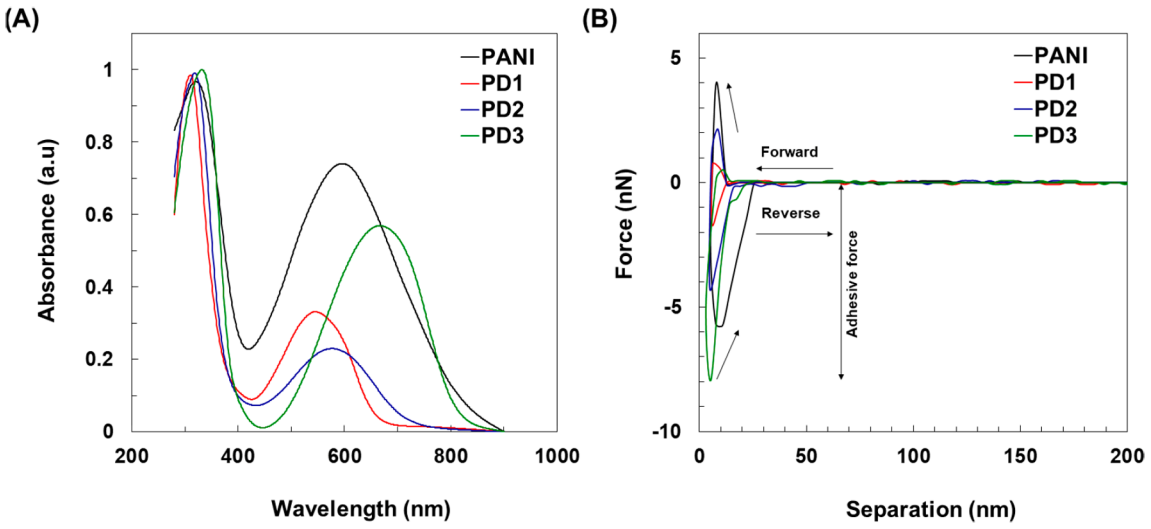

Figure 3. (A) UV−vis spectra of the various undoped polymers. (B) AFM force−distance curve of PANI, **PD1**, **PD2**, and **PD3**.

EDX analysis. Elemental analysis was performed by the X-max 80 EDX detector (Oxford Instruments) at 20 kV.

FTIR spectra were collected using a diamond ATR instrument (iD7 ATR-FTIR Nicolet iS5, ThermoFisher Scientific). Each spectrum is an average of 400 scans with a nominal resolution of 4 cm^{-1}. Raman spectra were acquired with a Yvon Horiba Raman spectrometer using a 632 nm laser source in microscope mode. UV−vis spectra of undoped polyaniline analogues and dedoped PANI were acquired with an Agilent Cary 60 spectrometer using a 1 cm quartz cell. The spectra of the polymer in NMP was corrected by subtracting the blank spectrum of NMP. Thermograms of the samples were acquired (TGA Q50 thermogravimetric analyzer, TA Instruments) under a N_2 flow of 20 mL/min and a heating rate of 10 °C/min. Contact angles were measured using a Tantec contact angle micrometer using the half-angle method. The coating thickness was measured by using a digital-readout caliper.

Electrochemical measurements were performed with a Solartron Analytical 1470E potentiostat/galvanostat using a three-electrode cell with a Ag/AgCl (saturated KCl) reference, a platinum auxiliary, and a steel coupon working electrode in 3.5 wt % aqueous NaCl electrolyte. The metal test electrode was mounted vertically with an exposed circular area of 12.8 cm^2. Potentiodynamic scans were from −0.25 to +0.25 V versus Ag/AgCl (saturated KCl) electrode about the open-circuit potential (OCP) at a scan rate of 0.2 mV s^{-1}. Multistat software (Scribner Associates) was used to acquire and evaluate the data. Electrochemical impedance spectroscopy (EIS) data were acquired from 100 mHz to 60 kHz with a 10 mV AC signal about the OCP using a Solartron SI 1250 frequency response analyzer. Impedance data were fitted to equivalent circuits with ZView 4.0 (Scribner Associates).

Accelerated corrosion tests were performed by exposing the samples for 24 h to a 6 wt % ferric chloride/0.1 M hydrochloric acid solution at 40 °C (ASTM G48-11).[36] Weight loss was determined after the sample was rinsed with deionized water and dried in a vacuum oven to a constant weight.

3. RESULTS AND DISCUSSION

3.1. ATR-IR Studies. ATR-IR spectra of **PD1**, **PD2**, **PD3**, and PANI are shown in Figures 2A and S10−S13. The broad peaks of the PANI spectrum at ≈3116−3426 cm^{-1} are attributed to stretching vibrations of the secondary amine N−H bond. The peaks at ≈3006−3093 cm^{-1} are attributed to the stretching of the aromatic C−H bond. The aliphatic C−H stretch is seen at ≈2813−2929 cm^{-1}.[31,37−40] Peaks at ≈1585 and ≈1495 cm^{-1} are attributed to the quinoid and benzenoid ring C═C bond stretch, respectively.[29,37,39,41] The C−N stretching vibration is assigned to ≈1217−1308 cm^{-1}.[32,41] The band at ≈1103−1163 cm^{-1} is attributed to −C−H in-plane bending for the 1,4-disubstituted aromatic ring, while the band appearing at ≈829 cm^{-1} can be assigned to the out-of-plane C−H bend in the benzenoid ring.[32,37,39]

Spectra of **PD1**, **PD2**, and **PD3** can be compared to PANI. The secondary amine N−H bond stretching vibration is present in all the three polyaniline analogues but not very prominent as they are very weak while the aromatic C−H stretching bond is more prominent in **PD1**, **PD2**, and **PD3** when compared to PANI. The quinoid ring C═C stretching peak near 1585 cm^{-1} is present in all the polymers.[27,42,43] Other major peaks of PANI are also present in the polyaniline analogues but with lower intensity. The imine (C═N) stretching peak is present in all the polymers at 1735 cm^{-1} for both **PD1** and **PD3** and 1739 cm^{-1} for PANI and **PD2**, respectively.

3.2. Raman Spectral Studies. Figures 2B and S14−S17 show the Raman spectra of PANI, **PD1**, **PD2**, and **PD3** in the range from 500 to 1700 cm^{-1}. The band at 1583 cm^{-1} in PANI corresponds to the C═N stretching vibration in the benzenoid ring, which was shifted to 1624, 1631, and 1627 cm^{-1} in **PD1**, **PD2**, and **PD3**, respectively.[3,44−46] The intense peak at 1481 cm^{-1} in PANI can be assigned to a C═C stretching vibration in the quinoid structures. This peak shifts to 1498, 1507, and 1496 cm^{-1} in **PD1**, **PD2**, and **PD3**, respectively.[3,45,46] The band of phenazine-like structures is assigned to 1328 cm^{-1} in PANI, 1405 cm^{-1} in **PD1** and **PD3**, and 1407 cm^{-1} in **PD2**. The band at 1321 cm^{-1} can be assigned to C−N^+ vibrations of delocalized polaronic structures in PANI. This peak is absent in **PD2** and very diminished in **PD1** (1308 cm^{-1}).[45] The C−N stretching vibration in **PANI** is assigned to the band at 1216 cm^{-1}, and the band at 1161 cm^{-1} was attributed to C−H bending vibration of quinonoid rings.[45] Both peaks are shifted to longer wavelengths and are much diminished in **PD1 to PD3**. The alterations in peak positions and intensities indicate the impact of electronic effects (inductive and mesomeric effects) from functional groups, underscoring the intricate interplay influencing the vibrational characteristics of the polymer.[47−49] The peaks at 840, 784, and 747 cm^{-1} observed in the PANI spectrum are attributed to benzene-ring deformations of substituted aromatic rings, which includes phenazine-like structures.[44,45,50] These peaks are also present in **PD1**, **PD2**, and **PD3** but again at longer wavelengths.

https://doi.org/10.1021/acsapm.3c02347
ACS Appl. Polym. Mater. 2024, 6, 3060−3072

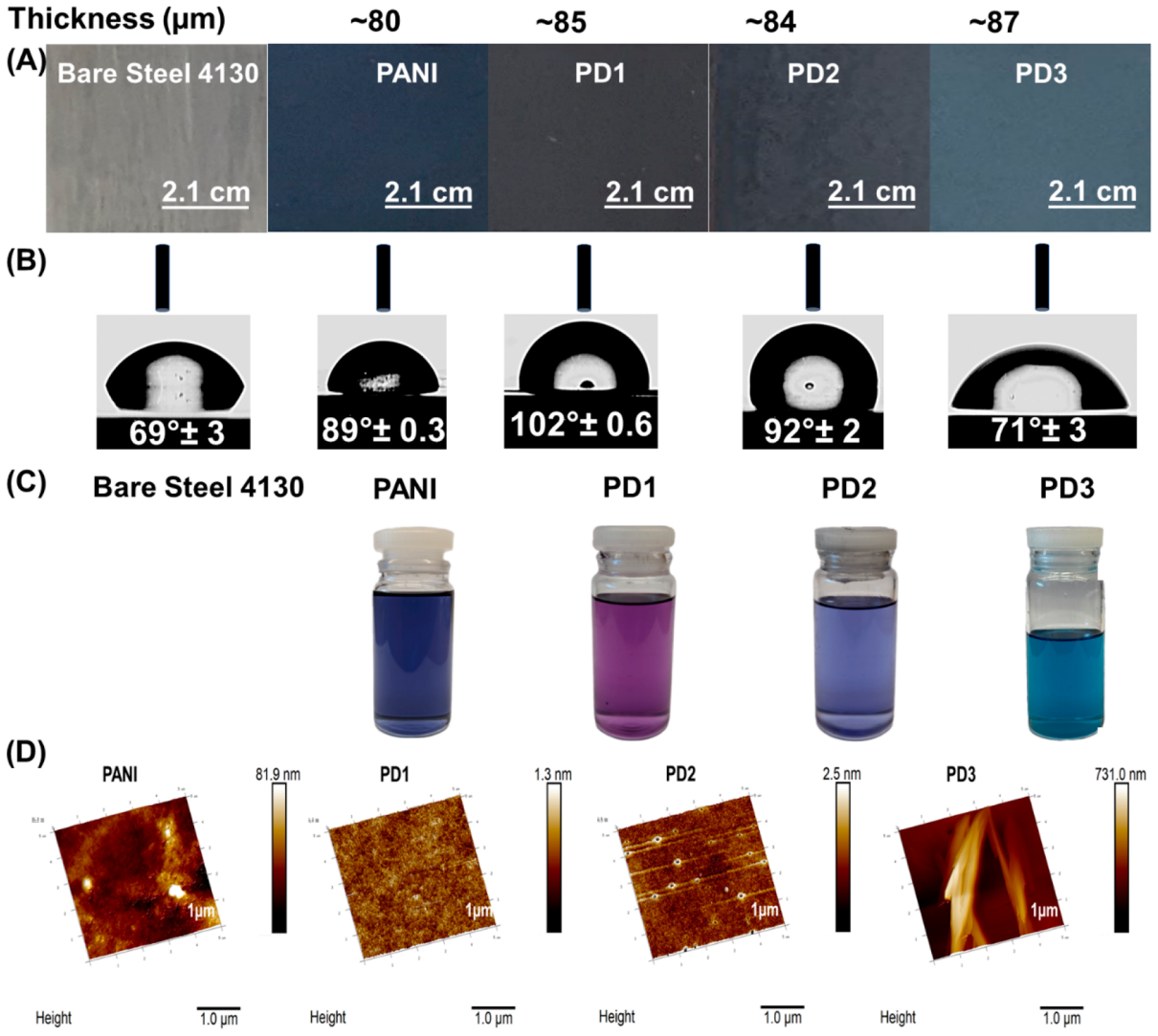

Figure 4. (A) Optical images of the uncoated AISI 4130 steel, PANI, and polyaniline analogue coated steels. (B) Static water contact angles of the polyaniline analogues. (C) Images of the polymers when dissolved in chloroform. (D) 3D AFM height images.

3.3. UV/Vis Spectroscopy. The UV−vis absorption spectra of PANI and polyaniline analogues (**PD1**−**PD3**) in chloroform are shown in Figure 3A. Strong peaks appear at 326 and 597 nm; 311 and 545 nm; 319 and 577 nm; and 333 and 668 nm for **PANI**, **PD1**, **PD2**, and **PD3**, respectively. The peaks from 311 to 333 nm indicate the $\pi-\pi^*$ transition in the benzenoid ring of the polymers, while the broad peaks of 545−668 nm for all the polymers have been assigned to the n−π^* transition from the benzenoid ring to the quinoid moiety of the polymers.[27,33,38,40,46] There is a hypsochromic shift in both the $\pi-\pi^*$ transitions in the benzenoid ring and the n−π^* transition from the benzenoid ring to the quinoid moiety for both **PD1** and **PD2** when compared to PANI. In contrast, a bathochromic shift is seen for both peaks of **PD3** compared to PANI.[27,40]

3.4. Thermogravimetric Analysis. Thermograms from thermogravimetric analysis (TGA) of **PD1**, **PD2**, **PD3**, and PANI under N_2 are shown in Figure S1. A small decrease in the weight of PANI below 100 °C is noted and assigned to dehydration and evaporation of absorbed water.[32,41,51] In general, the thermograms in Figure S1 suggest a one-stage weight loss process for all of the polymers except for PANI, which exhibits a two-step degradation process. PANI has the highest onset of decomposition temperature, T_d, at 474 °C, followed by **PD1** at 438 °C and **PD3** at 343 °C. In contrast, **PD2** has the lowest T_d onset at 343 °C. All the polyaniline analogues are thermally stable up to 350 °C. It was suggested in previous reports that the second degradation process of PANI at 600 °C is associated with the breaking of C−N, N−H, aromatic C−H bonds, and carbonization of aromatic rings, resulting in charring.[41,51,52] The thermal stability of the PANI analogues may arise from the rigidity of the fused ring systems in their structure.

3.5. Visual Images of the Samples and Contact Angle. Optical images of the uncoated and coated substrates are provided in Figure 4A. In a comparison of the color of the polymer-coated steel with a chloroform solution of the polymer, it is seen that the **PD1** coating is dark gray, while magenta color is seen in a chloroform solution (Figure 4C). **PD2** coatings are ash colored but are violet in chloroform. **PD3** is an ocean blue color as a coating and in an NMP solution. The **PD3** film coating is more brittle than the **PD1** and **PD2** coatings, implying

https://doi.org/10.1021/acsapm.3c02347
ACS Appl. Polym. Mater. 2024, 6, 3060−3072

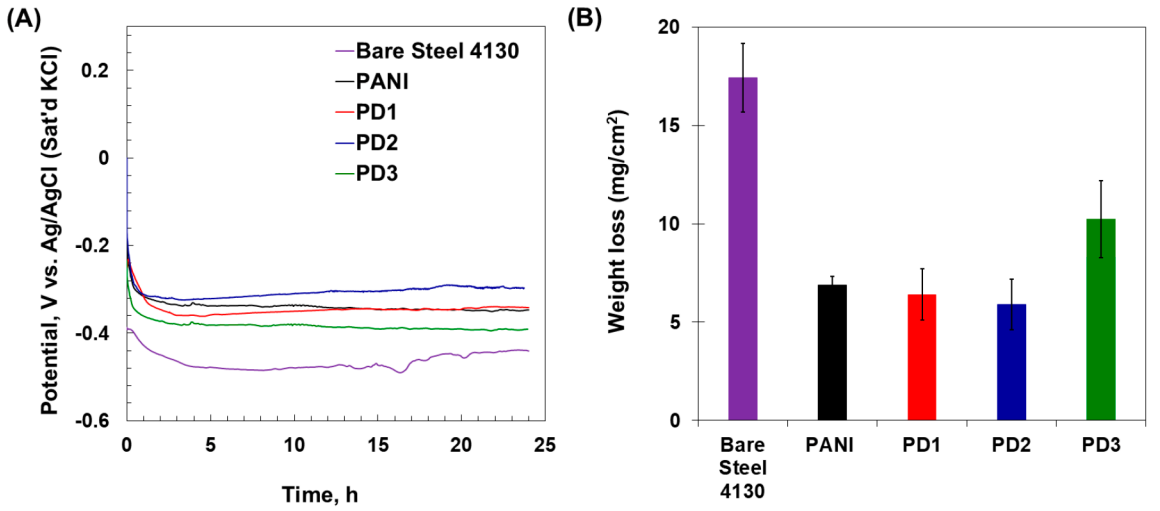

Figure 5. (A) Time-dependent OCP plots after 24 h of immersion in 3.5 wt % NaCl solution. (B) Weight losses of the substrates after 24 h immersion in 40 °C, 6 wt % $FeCl_3$/0.1 M HCl solution. The error bar indicates one SD, $n \geq 3$.

increased crystallinity. PANI is a dark blue amorphous coating on steel with a similar color when dissolved in NMP.

Thickness is an important factor in the efficiency of a barrier coating.[53] Improved barrier properties and corrosion resistance are found by optimizing coating thickness. The thickness of our coatings is estimated to be in the range 80−87 μm, which is significantly thinner than the ≈150 μm thickness typical of protective coatings used in industrial applications and compared well to similar studies.[53−58] Still, some demanding applications could call for thicker coatings. Thin coatings lead to more rapid failure than in a typical application. Contact angle (CA) measurements examined the wettability of the coated steels and the uncoated alloy steel samples (Figure 4B). Uncoated steel samples had a CA of 69 ± 3°, indicating a hydrophilic surface with a high surface energy. PANI-coated steels show a slightly higher CA of 89 ± 0.3°; this increase is likely due to nonpolar aromatic rings in the polyaniline structure. **PD1** was the most hydrophobic surface, with a CA value of 102°, again, due to nonpolar aromatic rings and alkyl groups within the matrix of the polymer. **PD2** has a contact angle of 92°. While **PD3** is hydrophilic with a CA value of 71°, it is likely from polar oxygen functional groups within the polymer. **PD1** is a carbazole without the second heteroatom, whereas **PD2** and **PD3** have S and O in their backbone, respectively.

3.6. Force−Distance Curve Analysis. The effect of the surface coating force required to withdraw an AFM (atomic force microscope) tip from our coated substrates is illustrated in Figure 3B. The adhesion force is directly proportional to the surface energy of the coated surface: an increased adhesion force indicates an increased surface energy, which is quantified by AFM.[59,60] Figure 3B shows the force−distance curves when an AFM cantilever tip approaches and retracts from the coated polyaniline (PANI) and polyaniline analogues (**PD1**, **PD2**, and **PD3**) surfaces in air. These curves reveal that **PD1** has the lowest maximum adhesion force of 1.68 ± 0.03 nN of **PD1** ($\mu \pm$ sd, $n \geq 3$) among the tested PANI analogues. The maximum adhesion forces for PANI, **PD2**, and **PD3** are approximately 5.69 ± 0.37, 4.20 ± 0.12, and 8.10 ± 1.49 nN, respectively. Compared to PANI, the low adhesion forces exhibited by the **PD2** and **PD3** coatings show that they have a lower surface energy and satisfactory nonstick behavior performance. The excellent result exhibited by carbazole-based **PD1** is likely due to the lack of electronegative atoms able to form hydrogen bonds with water. This result supports the data from the contact angle measurements.

AFM imaging is used to characterize the surface morphology and topography of the coated samples (Figures 4D, S2, and S3). **PD3** is distinct in showing a fibrous structure erupting from the surface (Figures 4D, S2, and S3). These features seen in **PD3** could be attributed to self-assembly and aggregation of the polymer strands during the synthesis or processing method used to prepare the polymer.[61−63] The AFM images of **PD3** show pores in the coating, perhaps due to solvent evaporation during film formation with this polymer. The AFM images show areas that resemble aggregated polymers that formed sheets with heights around 82, 1.3, 2.5, and 731 nm for PANI, **PD1**, **PD2**, and **PD3**, respectively (Figures 4D and S2). Surface roughness (R_{RMS}), average roughness (R_a), and the maximum peak depth to height are provided in Table S1. The **PD1** sample had the lowest R_{RMS} of 0.370, while **PD2** has the lowest maximum peak depth of 8.22 nm. **PD3** had the largest roughness of all of the coatings.

3.7. XRD Analysis. XRD data for **PD1**, **PD2**, **PD3**, and PANI are shown in Figure S4. The d spacing is found from Bragg's law (eq 1), and the crystallite size (D) was determined from the Scherrer equation (eq 2).

$$n\lambda = 2d \sin\theta \tag{1}$$

$$D = \frac{K\lambda}{\beta \cos\theta} \tag{2}$$

where Θ is the Bragg angle of the XRD peak, β is the width at half-maximum (FWHM) of crystallite peak (in radians), K is the shape factor for an average crystallite (0.94) depending on the Miller index of the reflecting plane and the shape of the crystal, and λ is the Cu Kα wavelength (here 0.154 nm), giving D, the crystallite size, in nm. The crystallite size of PANI is found to be 1 nm, while those of **PD1**, **PD2**, and **PD3** are 2 nm each (Table S2). This confirms the formation of PANI nanofibers and nanofibers for the synthesized polyaniline analogues.

The percentage crystallinity in the PANI nanofibers is 17.04%, implying that the undoped polyaniline is mainly amorphous. This agrees with earlier reports that emeraldine base polyaniline

https://doi.org/10.1021/acsapm.3c02347
ACS Appl. Polym. Mater. 2024, 6, 3060−3072

is an amorphous polymer.[32,64−66] The polyaniline analogues are also mainly amorphous polymers with crystallinity ranging from 15% (**PD1**) to 23% (**PD3**). The repeating benzenoid and quinoid moieties in these polymers is responsible for their high amorphicity.[32]

The broad diffraction peaks between 5° and 30° seen in all the polyaniline and polyaniline analogues have been attributed to the periodicity parallel and perpendicular to the polyaniline chain in the polymers.[30,32,67] Figure S4 shows the diffracted PANI peaks with their corresponding d-spacing at $2\theta = 9.5953°$ ($d = 9.2110$ Å), 18.7119° ($d = 4.7383$ Å), 23.4108° ($d = 3.7968$ Å), and 40.2769° ($d = 2.2374$ Å), as reported previously.[31,66,68,69] **PD1** shows 2 reflections at $2\theta = 8.2475°$ and 20.2635° with corresponding interplanar distances of d = 10.7119 and 4.3789 Å. Overall, the polyaniline analogues gave similar diffraction patterns to PANI except for **PD1** with a significantly lower peak in relation to PANI. Table S2 shows the peak angles and their corresponding d-spacings.

3.8. Electrochemical Measurements/Corrosion Studies. Results from the OCP, potentiodynamic polarization, and EIS tests are discussed below.

3.8.1. Open-Circuit Potential Measurements. Figure 5A shows the variation in open-circuit potential (OCP) during a 24 h period after immersion of the samples in 3.5 wt % NaCl solution. OCP values of the PANI and polyaniline analogues are more positive than the uncoated steels ($\mu \pm 95\%$ confidence interval, $n \geq 3$, and % relative standard deviation RSD $\leq 5\%$).

The potentials at 24 h are −442 ± 6, −344 ± 27, −342 ± 42, −326 ± 30, and −385 ± 21 mV for bare steel 4130, PANI, **PD1**, **PD2**, and **PD3**, respectively. After an initial negative shift, the OCP values stabilized to distinct values, with all the polymers settling to values more positive than bare steel. This positive OCP shift (i.e., in the noble direction) is an indication of a lower corrosion susceptibility. **PD2** has the largest shift; at about 116 mV more positive than the uncoated steel substrate. The polyaniline analogues contain cross-linked aryl and alkyl groups within its structure reducing their permeability and rate of electrolyte uptake.[70] Thus, the coatings exhibit a passivation effect, forming a protective layer on the substrates resulting in higher OCP values and high resistance to a corrosive media.[6]

3.8.2. Tafel Test/Potentiodynamic Polarization Test. Potentiodynamic polarization testing was done after the 24 h of the OCP experiment to indicate the anticorrosion performance of the samples. Tafel plots—plots of potential against the logarithm of the current density (log J) are shown in Figure 6. The corrosion potential (E_{corr}) and corrosion current (I_{corr}) values are extracted by fitting the Tafel plot to the Butler−Volmer equation.[71] The protection efficiency (PE%) estimates the ability of the coating to minimize corrosion and is calculated from eq 3.

$$\text{PE}\ (\%) = \frac{I_{corr,uc} - I_{corr,c}}{I_{corr,uc}} \times 100 \tag{3}$$

where $I_{corr,uc}$ and $I_{corr,c}$ are the corrosion current densities of the uncoated and coated samples. The corrosion parameters extracted from the Tafel plots are given in Table 1.

As expected, the uncoated substrate displays significantly higher cathodic and anodic current values compared to the coated substrates (**PD1**, **PD2**, **PD3**, and PANI). Lower metal corrosion rates are indicated by smaller I_{corr} values. Additionally, as in the OCP tests, a more positive E_{corr} value implies a smaller corrosion tendency.[72] The E_{corr} values of the uncoated substrate are more negative than those of the coated substrates. Organic coatings may not always provide the best barrier against corrosive media, but the diffusion pathways of coatings made of higher density materials or polymers with cross-linked structures are more constrained, resulting in a lower permeability. Higher OCP values and greater tolerance to corrosive environments are outcomes of this lower permeability.[73−75] Further, data from contact angle and AFM adhesion tests show that PANI and PANI analogues possess low surface energy and act as a hydrophobic barrier to diffusion of the corrosive electrolytes across the coating-metal surface. **PD2** has the most positive E_{corr} at −300 ± 6.6 mV and the smallest I_{corr} value at 0.129 ± 0.11 μA/cm^2, giving this material a PE% value of 95.9%—higher than the PANI coating. In contrast, **PD3** with an I_{corr} value of 1.656 ± 0.16 μA/cm^2, and an E_{corr} value of −343.7 ± 10.69 mV has a PE % value of 47.6%, performing well below PANI and the other polyaniline analogue polymers. These results indicate that **PD1** and **PD2** should perform better than PANI in anticorrosion applications.

3.9. SEM/EDX Analysis. Figure 7 shows the morphologies of the samples before and after 24 h exposure to 3.5 wt % NaCl solution. Corresponding EDX spectra are also presented in Figure S5. The EDX spectrum showed peaks for Fe, C, Cr, Al, Si, Ti, and Mn elements present in the bare and coated steel samples. The presence of Fe, C, Cr, and Mn peaks in the EDX spectrum of the coated substrates is due to the ability of the high-energy electron beams to penetrate the coating and interact with the metal surface. Pt is present from the conductive Pt coatings applied to the substrates to avoid charging artifacts during SEM. The EDX spectra of **PD2** and **PD3** additionally had S and O peaks, respectively, from the polymer composition.

After 24 h exposure to the 3.5% NaCl solution, uncoated steel shows irregular pores with deep cavities on the surface media due to corrosion.[40] Prior to exposure, the surface is smooth, showing only polishing scratches. The EDX spectrum indicates an increase in O on the postexposure sample.

In the coated samples, the ability of polyaniline to reduce corrosion rate is attributed to the interaction of metallic cations with the imine nitrogen atom in PANI, which produces a change in the morphology and structure of PANI.[15,24] This change is evident in the SEM of PANI before and after exposure to NaCl; the initial feathery structures condense to a more cohesive film after exposure. Some delamination of the PANI coating is also noted after immersion in NaCl solution for 24 h. **PD1** produces a uniform and very smooth layer on steel surfaces. However, the film typically forms cracks a few days after **PD1** coatings were

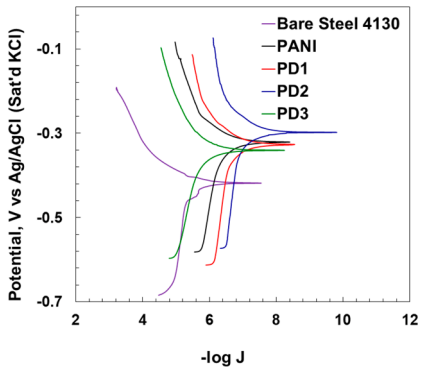

Figure 6. Tafel plot after 24 h of immersion in 3.5 wt % NaCl solution.

https://doi.org/10.1021/acsapm.3c02347
ACS Appl. Polym. Mater. 2024, 6, 3060−3072

Table 1. Corrosion Parameters Extracted from the Tafel Plots

	bare steel	PANI	PD1	PD2	PD3
I_{corr} (μA/cm^2)	3.16 ± 0.62	0.38 ± 0.17	0.35 ± 0.19	0.13 ± 0.11	1.66 ± 0.16
E_{corr} (mV vs Ag/AgCl (satd))	−413 ± 4	−335 ± 13	−338 ± 17	−300 ± 7	−344 ± 11
corrosion rate (μm / year)	37.5	4.6	4.1	1.5	19.7
protection efficiency (%)		87.8	89.0	95.9	47.6

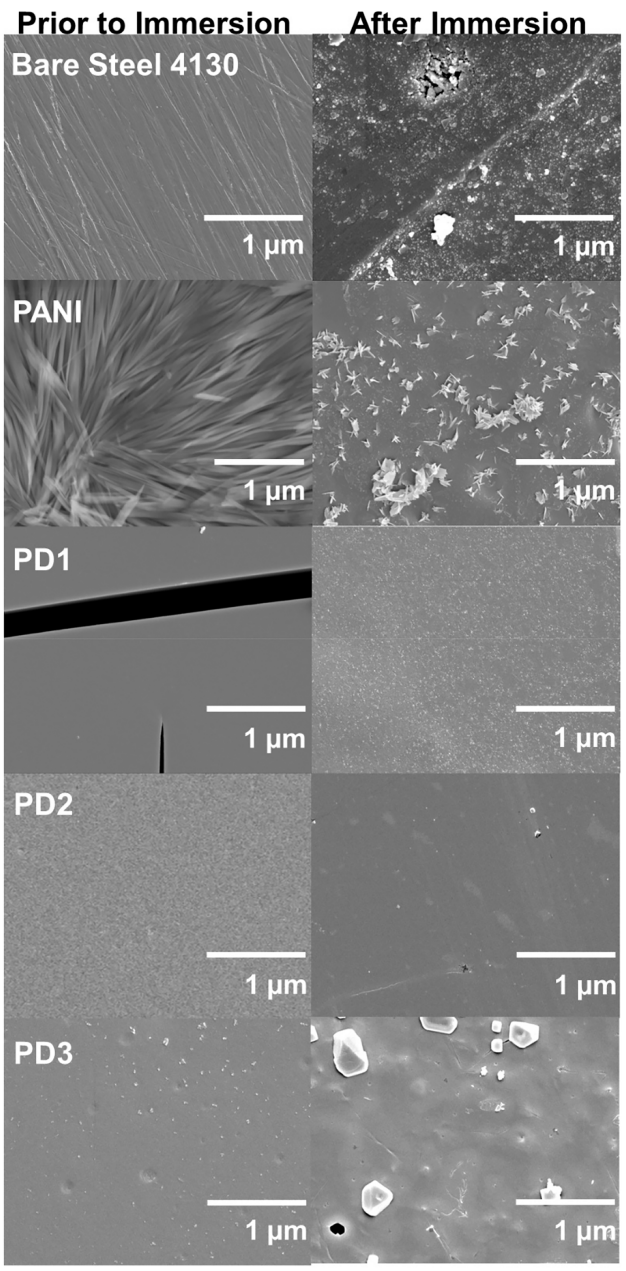

Figure 7. SEM pattern of uncoated steels, PANI, **PD1**, **PD2**, and **PD3** before and after 24 h of exposure to NaCl solution.

applied, as seen in the SEM. Only a slight roughening of the **PD1** surface is noted after exposure to 24 h of NaCl. The coated surface also only showed slight surface changes seen after immersion in NaCl. In contrast, the **PD3** surface shows the presence of corrosion products (i.e., lighter particles seen on the surface of the polymer) and pits after exposure. There is also a change in the surface texture of **PD3**, which can be attributed to the absorption and percolation of water into the coating, resulting in swelling. The EDX spectrum for **PD3**, postexposure, shows a large increase in Cl, likely due to the presence of chloride-containing corrosion products.[76] In contrast, **PD1** and **PD2** coatings show only minimal formation of white corrosion product particles and pits after 24 h in corrosive media.

3.10. EIS Study. An EIS study was used to understand the electrochemical behavior and anticorrosion performance of the polyaniline analogues on AISI 4130 steel in 3.5 wt % NaCl solution.[2,33] EIS data were acquired by excitation with a 10 mV rms sine wave over the frequency range of 0.1 Hz−60 kHz. Figures 8A−E show the Nyquist plots (real impedance Z' vs the imaginary impedance Z'') of bare AISI 4130 steel and various coatings. The uncoated steel shows a single depressed semicircle in Figure 8A. The depressed semicircle indicates an imperfect capacitance with a resistive component. The Nyquist plots for **PANI**, **PD1**, **PD2**, and **PD3** coated substrates in Figures 8B−E also contain depressed semicircles in the high-frequency region and an incomplete semicircle at low frequency.

A Randles electrical model (Figure 8F, model A) with solution resistance (R_s) in series with a parallel constant phase element (CPE_{dl}-T) and charge-transfer resistance R_{ct} (or polarization resistance R_p) element provides a good fit to the bare steel sample. A constant phase element (CPE) is used to model the nonideal behavior of the double-layer capacitor.[2,77] The impedance of the CPE is

$$Z_{CPE} = \frac{1}{(2j\pi f)^n Y_0} \quad (4)$$

where Y_0 is the capacitance; n accounts for the nonideal behavior of the capacitor and ranges from n = 1 (purely capacitive) to 0.[2,23,77,78]

The simple Randles model is inadequate for the coated substrates. Thus, there is a need to account for the heterogeneity of the protective coating and mass transfer processes producing time constant variations and other deviations.[2,28,53,79−81] The two electrochemical interphases that exist between the substrate surface and the electrolyte solution were accounted for by model B in Figure 8F. The charge transfer at the interphase between the metal and the coat is represented by R_{ct}−(CPE_{dl}-T), while the coating interphase is accounted for by R_c−(CPE_c-T). The model thus accounts for the two-time constants observed in the experimental Bode magnitude (log |Z| vs log f) and phase angle (θ vs log f) plots for the bare steel and the coated steels which are displayed in Figure S6.[53,76,81] The region above 1 kHz in the Bode magnitude and the phase angle plots gives the coating barrier performance, while the formation of corrosion products, due to failure of the barrier coatings, is indicated below 1 kHz.[28,53,82,83]

Electrochemical parameters from fitting the EIS data to the models are listed in Table 2. Note that R_s for the bare steel was 19 ± 0.56 Ω cm^2, which was much lower than the other samples, reflecting an increase in ion concentration in solution as the metal corrodes. At low frequencies, the impedance modulus (|Z|) for bare steel is 141.7 ± 1.1 Ω cm^2, which is very small. The bare steel exhibited a single time constant below 10 Hz, arising

https://doi.org/10.1021/acsapm.3c02347
ACS Appl. Polym. Mater. 2024, 6, 3060−3072

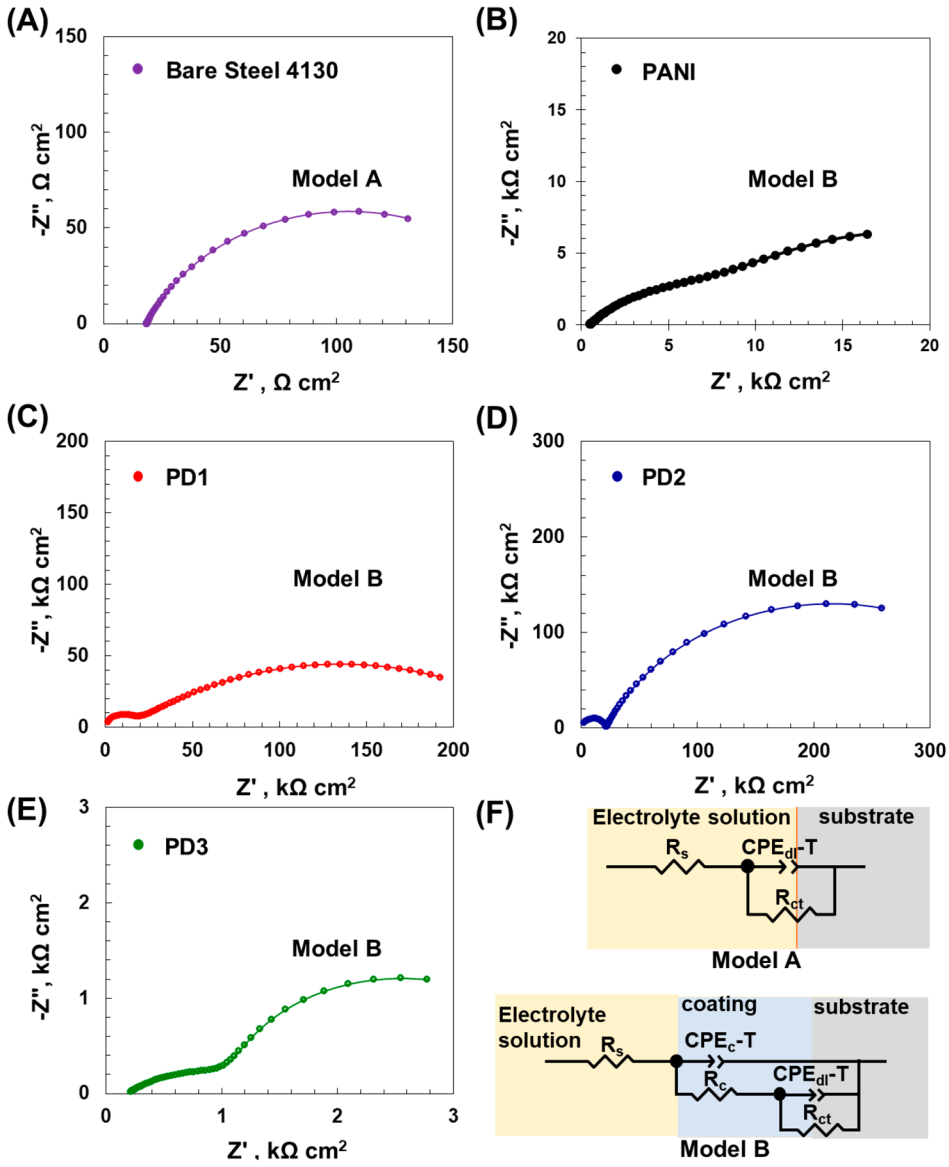

Figure 8. Nyquist plots for (A) bare steel 4130, (B) PANI, (C) **PD1**, (D) **PD2**, and (E) **PD3** and (F) equivalent electrical circuit (EEC) models.

Table 2. EIS Parameter Values Obtained from Fitting the EIS Data of the Uncoated and Coated Substrates after 24 h Immersion in 3.5 wt % NaCl Solution

	bare steel 4130	PANI	PD1	PD2	PD3
R_s (Ω cm^2)	19 ± 0.6	450 ± 6	550 ± 20	570 ± 10	190 ± 4
CPE_c-T					
Y_0 ($\mu\Omega^{-1}$ s^n cm^{-2})		14 ± 1.3	(7.2 ± 0.5) × 10^{-4}	(6.3 ± 0.9) × 10^{-4}	108 ± 4
n		0.55 ± 0.01	0.99 ± 0.01	0.97 ± 0.01	0.43 ± 0.01
R_c (kΩ cm^2)		11.0 ± 0.9	15.0 ± 0.4	21 ± 2.1	1.3 ± 0.04
CPE_{dl}-T					
Y_0 (mΩ^{-1} s^n cm^{-2})	4.7 ± 0.46	(6.8 ± 0.09) × 10^{-2}	(1.9 ± 0.5) × 10^{-2}	(2.3 ± 0.5) × 10^{-3}	0.24 ± 0.01
n	0.75 ± 0.01	0.63 ± 0.01	0.45 ± 0.02	0.75 ± 0.01	0.93 ± 0.02
R_{ct} (kΩ cm^2)	0.17 ± 0.01	20 ± 2.2	240 ± 49	390 ± 38	3.3 ± 0.19
χ^2	2.4 × 10^{-4}	1.5 × 10^{-3}	8.3 × 10^{-4}	2.7 × 10^{-4}	2.6 × 10^{-3}

from the formed metallic oxide layer. The polymer-coated samples show much higher R_s, indicating a small increase in the number of ions present in the electrolyte solution due to corrosion. The parallel combination of R_{ct} and CPE_{dl}-T, which models the electrochemical reaction occurring at the coating–metal interface in model B, estimates the electron transfer rate between the coatings and the metal. A lower R_{ct} value implies a high electron transfer rate.[2] The R_{ct} value for the bare steel was 0.17 ± 0.01 kΩ cm^2 while higher values of 20 ± 2.2, 240 ± 49, and 390 ± 38 kΩ cm^2 were obtained for PANI, **PD1**, and **PD2**,

https://doi.org/10.1021/acsapm.3c02347
ACS Appl. Polym. Mater. 2024, 6, 3060−3072

respectively. **PD2** and **PD1** gave a superior barrier performance, with |*Z*| values of 2.9 ± 0.9 and 2.0 ± 0.3 MΩ cm^2, respectively, when compared to **PD3** and even **PANI** with a |*Z*| value of 17.6 ± 6.1 kΩ cm^2. **PD2** and **PD1** have lower θ values of −26° and −10°, respectively, at low frequencies, which suggests minimal coating damage. At high frequency, both **PD2** and **PD1** have phase angles of −65° and −68°, respectively. This implies that the coatings reduce the corrosion rate of the substrates in the corrosive media. **PD3** has two time constants: one at a mid-frequency due to the protective ability of the polymer and another time constant at low frequency with a |*Z*| value of 3.0 ± 0.3 kΩ cm^2 with phase angle (θ) = −23°, indicating minimal coating damage. **PD3** gave low resistance values, indicating poor corrosion protection. Studies have revealed that lower values of CPE$_{dl}$-*T* predict lowered corrosion rates, indicating a reduction in the distribution of electrical charges between the metal−solution interphase, thus delaying the production and dissolution of hydrophilic corrosion products (e.g., hydrated metal oxides and hydroxides).[28,82−84] The R_c values of the coated samples tracks the R_{ct} values. Larger R_c values can delay the movement of corrosive electrolytes to the metallic substrate. **PD1** and **PD2** display larger R_c values and lower CPE$_c$-*T* values [(7.2 ± 0.5) × 10^{-4} and (6.3 ± 0.9) × 10^{-4} $\mu\Omega^{-1}$ s^n cm^{-2}] when compared to **PD3** and even PANI. This is consistent with the lack of major damage and evidently low water absorption in the coatings after exposing the coated substrates to the corrosive media, as noted in the SEM images (Figure 7), where in comparison, the surface texture of **PD3** looks swollen.[77,82] The increase in rigidity from the carbazole and the phenothiazine cores in **PD1** and **PD2** may account for the reduction of porosity—reducing the percolation of ions through the coating.[27,35] The use of these polymers as coating barriers helps to increase the impedance modulus values. In contrast, the low R_c (1.28 ± 0.04 kΩ cm^2) and much higher CPE$_c$-*T* (108.3 ± 3.9 $\mu\Omega^{-1}$ s^n cm^{-2}) values of **PD3** support water adsorption producing the change in the surface texture of the coating in the SEM image (Figure 7) after being exposed to the corrosive media. This EIS result agrees with the data from the OCP and Tafel experiment where both **PD1** and **PD2** gave a superior performance in comparison to PANI and **PD3** coatings.

3.11. Accelerated Corrosion Test. An accelerated corrosion test was performed by immersing the coated substrates in an aggressively corrosive solution of 6 wt % $FeCl_3$ in 0.1 M HCl at 40 °C to evaluate the robustness of the coatings and their resistance on long-term use in an aggressive electrolyte solution.[36] Figure 5B shows the mass loss of these substrates after 24 h immersion in this solution.

The results support the potentiodynamic, EIS, and SEM/EDX experiments. The high weight loss of 10.2 mg cm^{-2} of **PD3** is consistent with the damage seen in the SEM image (Figure 7) after exposure to the less aggressive NaCl solution. The poor performance of **PD3** may be ascribed to hydrolysis of weakly bound O atoms in the phenoxazine-based polyaniline analogue polymers, thus doping the polymer, which initiates damage of the polymer coating, noted by the presence of corrosion products, crevices, and cracks appearing on the coated surface.[53] The lowest weight loss of 5.9 mg cm^{-2} in **PD2** may be due to the presence of a C−S bond in the polymer matrix, which makes its bond less polar compared to the C−O bonds in the phenoxazine polymer. These phenothiazine-based polyaniline analogues display superior barrier property as it delays corrosion of the substrates.

4. CONCLUSIONS

Our initial study of polyaniline analogues as corrosion-protection coatings has demonstrated that they offer a noticeable enhancement of corrosion protection for AISI 4130 steel in 3.5 wt % NaCl. The phenothiazine and carbazole based polyaniline analogues performed nearly as well as the commercial polymer PANI with this initial corrosion testing. The carbazole and phenothiazine (**PD1** and **PD2**) based polymers are good hydrophobic barriers to protect metal surfaces from ingress of corrosive media. Based on this investigation, these polymers provide low corrosion rates, high impedance values from the EIS, and very high protection efficiency. Results from the Tafel plot, EIS, SEM/EDS, AFM, and accelerated corrosion test support the observations seen with 24 h immersion times used in related studies.[3,24,40,53,55−58,85,86] The superior performance of corrosion resistance in the carbazole and phenothiazine based polymers might be attributed to the absence of polar functional groups and the presence of nonpolar covalent bonds (e.g., C−C, C−H, and C−S bonds for phenothiazine), which increases hydrophobicity, corrosion resistance, and stability in aggressive media. **PD1** and **PD2** can be used as standalone barrier coatings due to their good adhesion and hydrophobicity. **PD3**, on the other hand, with lower impedance values, can serve as a primer for contributing to enhanced corrosion resistance within a comprehensive paint matrix. All the polymers may also find use as additives to paint primer coatings to enhance corrosion resistance of the paint matrix. **PD1** and **PD2** have the highest corrosion resistance among the tested PANI analogues in this study and may prove valuable as an alternative polymeric barrier coating. Further investigation into their suitability will require the production of thinner coatings to match commercial applications. Moreover, we must investigate protection over longer terms with prolonged exposure to corrosive media and accelerated aggressive corrosion testing (e.g., the salt−fog method) to validate this assertion. In addition, enhancement of the protective ability of these polymers will be investigated by adding nanofillers and additives (such as montmorillonite, silica, carbon nanotubes, graphene oxide, titania, etc.), which are likely to act as barriers by increasing tortuosity against electrolyte intrusion, further improving corrosion, adhesion, and mechanical protection. All the PANI analogues were studied in their undoped nonconductive state. As with PANI, there may be significant advantages to using these polymers in their conducting state, such as particulate additives to paint, epoxy, or primer formulations.[33,87]

■ ASSOCIATED CONTENT

Supporting Information

The Supporting Information is available free of charge at https://pubs.acs.org/doi/10.1021/acsapm.3c02347.

Thermograms of the polymers; XRD pattern of the polymers; EDX pattern of the bare steel and the uncoated steels; AFM images of coated images; Bode magnitude and phase angle plots of the bare and coated steel; calculation of the equivalent weight of AISI 4130 steel; calculation for corrosion rate from corrosion current; ^{1}H NMR spectra of **PD1**, **PD2**, and **PD3**; ATR-IR spectrum of **PD3** (PDF)

https://doi.org/10.1021/acsapm.3c02347
ACS Appl. Polym. Mater. 2024, 6, 3060−3072

AUTHOR INFORMATION

Corresponding Author

David O. Wipf − *Department of Chemistry, Mississippi State University, Mississippi State, Mississippi 39762, United States;* orcid.org/0000-0003-2365-1175; Email: DWipf@chemistry.msstate.edu

Authors

Raymond Femi Awoyemi − *Department of Chemistry, Mississippi State University, Mississippi State, Mississippi 39762, United States*

Mohammed Almtiri − *Department of Chemistry, Mississippi State University, Mississippi State, Mississippi 39762, United States*

Hari Giri − *Department of Chemistry, Mississippi State University, Mississippi State, Mississippi 39762, United States*

Colleen N. Scott − *Department of Chemistry, Mississippi State University, Mississippi State, Mississippi 39762, United States;* orcid.org/0000-0003-3332-2439

Complete contact information is available at: https://pubs.acs.org/10.1021/acsapm.3c02347

Author Contributions

R.F.A.: conceptualization, investigation, data curation, writing−original draft, visualization, writing−review and editing. M.A.: investigation, writing−review and editing. H.G.: investigation, data curation, writing−review and editing. C.N.S.: writing−review and editing supervision, resources. D.O.W.: writing−review and editing, supervision, resources.

Funding

The authors acknowledge financial support from the National Science Foundation (CHE-1945503).

Notes

The authors declare no competing financial interest.

ACKNOWLEDGMENTS

The authors thank Bruno Donnadieu, Dr. Sumudu Athakuramole, and Dr. Iwei Chu (I^2AT) for their help in acquiring the XRD spectra, Raman spectroscopy, AFM, and SEM/EDX, respectively.

REFERENCES

(1) Heeger, A. J. Nobel Lecture: Semiconducting and Metallic Polymers: The Fourth Generation of Polymeric Materials. *J. Phys. Chem. B* **2001**, *105* (36), 8475−8491.

(2) Deshpande, P. P.; Sazou, D. *Corrosion Protection of Metals by Intrinsically Conducting Polymers*; CRC Press Taylor & Francis Group: Boca Raton, FL, 2016.

(3) Madhan Kumar, A.; Gasem, Z. M. In Situ Electrochemical Synthesis of Polyaniline/f-MWCNT Nanocomposite Coatings on Mild Steel for Corrosion Protection in 3.5% NaCl Solution. *Prog. Org. Coat.* **2015**, *78*, 387−394.

(4) Spinks, G. M.; Dominis, A. J.; Wallace, G. G.; Tallman, D. E. Electroactive Conducting Polymers for Corrosion Control. *J. Solid State Electrochem.* **2002**, *6* (2), 85−100.

(5) Tallman, D. E.; Spinks, G.; Dominis, A.; Wallace, G. G. Electroactive Conducting Polymers for Corrosion Control Part 1. General Introduction and a Review of Non-Ferrous Metals. *J. Solid State Electrochem.* **2002**, *6*, 73−84.

(6) Abu-Thabit, N. Y.; Makhlouf, A. S. H. Recent Advances in Polyaniline (PANI)-Based Organic Coatings for Corrosion Protection. In *Handbook of Smart Coatings for Materials Protection*; Makhlouf, A. S. H., Ed.; Elsevier: 2014; pp 459−486.

(7) Namsheer, K.; Rout, C. S. Conducting Polymers: A Comprehensive Review on Recent Advances in Synthesis, Properties and Applications. *RSC Adv.* **2021**, *11* (10), 5659−5697.

(8) Nezakati, T.; Seifalian, A.; Tan, A.; Seifalian, A. M. Conductive Polymers: Opportunities and Challenges in Biomedical Applications. *Chem. Rev.* **2018**, *118* (14), 6766−6843.

(9) Mrad, M.; Amor, Y. B.; Dhouibi, L.; Montemor, F. Electrochemical Study of Polyaniline Coating Electropolymerized onto AA2024-T3 Aluminium Alloy: Physical Properties and Anticorrosion Performance. *Synth. Met.* **2017**, *234*, 145−153.

(10) Mrad, M.; Dhouibi, L.; Triki, E. Dependence of the Corrosion Performance of Polyaniline Films Applied on Stainless Steel on the Nature of Electropolymerisation Solution. *Synth. Met.* **2009**, *159* (17), 1903−1909.

(11) DeBerry, D. W. Modification of the Electrochemical and Corrosion Behavior of Stainless Steels with an Electroactive Coating. *J. Electrochem. Soc.* **1985**, *132* (5), 1022−1026.

(12) Cecchetto, L.; Ambat, R.; Davenport, A. J.; Delabouglise, D.; Petit, J. P.; Neel, O. Emeraldine Base as Corrosion Protective Layer on Aluminium Alloy AA5182, Effect of the Surface Microstructure. *Corros. Sci.* **2007**, *49* (2), 818−829.

(13) Gonçalves, G. S.; Baldissera, A. F.; Rodrigues, L. F.; Martini, E. M. A.; Ferreira, C. A. Alkyd Coatings Containing Polyanilines for Corrosion Protection of Mild Steel. *Synth. Met.* **2011**, *161* (3−4), 313−323.

(14) Mathew, A. M.; Predeep, P. Styrene Butadiene Co-Polymer Based Conducting Polymer Composite as an Effective Corrosion Protective Coating. *Prog. Org. Coat.* **2012**, *74* (1), 14−18.

(15) Sathiyanarayanan, S.; Karpakam, V.; Kamaraj, K.; Muthukrishnan, S.; Venkatachari, G. Sulphonate Doped Polyaniline Containing Coatings for Corrosion Protection of Iron. *Surf. Coat. Technol.* **2010**, *204* (9−10), 1426−1431.

(16) Cecchetto, L.; Delabouglise, D.; Petit, J. P. On the Mechanism of the Anodic Protection of Aluminium Alloy AA5182 by Emeraldine Base Coatings: Evidences of a Galvanic Coupling. *Electrochim. Acta* **2007**, *52* (11), 3485−3492.

(17) Nguyen, T. D.; Nguyen, T. A.; Pham, M. C.; Piro, B.; Normand, B.; Takenouti, H. Mechanism for Protection of Iron Corrosion by an Intrinsically Electronic Conducting Polymer. *J. Electroanal. Chem.* **2004**, *572* (2), 225−234.

(18) Stejskal, J.; Kratochvíl, P.; Jenkins, A. D. Polyaniline: Forms and Formation. *Collect Czechoslov Chem. Commun.* **1995**, *60* (10), 1747−1755.

(19) Malhotra, B.; Dhand, C.; Lakshminarayanan, R.; Dwivedi, N.; Mishra, S.; Solanki, P.; Venkatesh, M.; Beuerman, R. W; Ramakrishna, S. Polyaniline-Based Biosensors. *Nanobiosensors in Disease Diagnosis* **2015**, *4*, 25−46.

(20) Duić, L.; Mandić, Z. Counter-Ion and PH Effect on the Electrochemical Synthesis of Polyaniline. *J. Electroanal. Chem.* **1992**, *335* (1−2), 207−221.

(21) Wei, Y.; Hsueh, K. F.; Jang, G.-W. Monitoring the Chemical Polymerization of Aniline by Open-Circuit-Potential Measurements. *Polymer (Guildf)* **1994**, *35* (16), 3572−3575.

(22) König, U.; Schultze, J. W. Kinetics of Polyaniline Formation and Redox Processes1. *J. Electroanal Chem. Interfacial Electrochem* **1988**, *242* (1−2), 243−254.

(23) Caldona, E. B.; de Leon, A. C. C.; Pajarito, B. B.; Advincula, R. C. Novel Anti-Corrosion Coatings from Rubber-Modified Polybenzoxazine-Based Polyaniline Composites. *Appl. Surf. Sci.* **2017**, *422*, 162−171.

(24) Abaci, S.; Nessark, B. Characterization and Corrosion Protection Properties of Composite Material (PANI+TiO_2) Coatings on A304 Stainless Steel. *J. Coat. Technol. Res.* **2015**, *12* (1), 107.

(25) Babel, V.; Hiran, B. L. A Review on Polyaniline Composites: Synthesis, Characterization, and Applications. *Polym. Compos* **2021**, *42* (7), 3142−3157.

(26) Kobayashi, T.; Yoneyama, H.; Tamura, H. Polyaniline Film-Coated Electrodes as Electrochromic Display Devices. *J. Electroanal Chem. Interfacial Electrochem* **1984**, *161* (2), 419−423.

(27) Almtiri, M.; Dowell, T. J.; Chu, I.; Wipf, D. O.; Scott, C. N. Phenoxazine-Containing Polyaniline Derivatives with Improved Electrochemical Stability and Processability. *ACS Appl. Polym. Mater.* **2021**, *3* (6), 2988.
(28) Yazdi, E. G.; Ghahfarokhi, Z. S.; Bagherzadeh, M. Protection of Carbon Steel Corrosion in 3.5% NaCl Medium by Aryldiazonium Grafted Graphene Coatings. *New J. Chem.* **2017**, *41* (21), 12470−12480.
(29) Al-Dulaimi, A. A.; Hashim, S.; Khan, M. I. Corrosion Protection of Carbon Steel Using Polyaniline Composite with Inorganic Pigments (Perlindungan Kakisan Keluli Karbon Menggunakan Komposit Polianilin Dengan Pigmen Inorganik). *Sains Malays* **2011**, *40* (7), 757−763.
(30) Shi, li; Wang, X.; Lu, L.; Yang, X.; Wu, X. Preparation of TiO_2/Polyaniline Nanocomposite from a Lyotropic Liquid Crystalline Solution. *Synth. Met.* **2009**, *159* (23−24), 2525−2529.
(31) Ajeel, K. I.; Kareem, Q. S. Synthesis and Characteristics of Polyaniline (PANI) Filled by Graphene (PANI/GR) Nano-Films. *J. Phys. Conf Ser.* **2019**, *1234*, No. 012020.
(32) Mostafaei, A.; Zolriasatein, A. Synthesis and Characterization of Conducting Polyaniline Nanocomposites Containing ZnO Nanorods. *Progress in Natural Science: Materials International* **2012**, *22* (4), 273−280.
(33) Qiu, S.; Chen, C.; Cui, M.; Li, W.; Zhao, H.; Wang, L. Corrosion Protection Performance of Waterborne Epoxy Coatings Containing Self-Doped Polyaniline Nanofiber. *Appl. Surf. Sci.* **2017**, *407*, 213−222.
(34) Liangcai, L.; Ming, W.; Huoming, S.; Haiying, L.; Qingdong, Q.; Yuanlong, D. Preparation and EIS Studies on Polyimide/Polyaniline Blend Film for Corrosion Protection. *Polym. Adv. Technol.* **2001**, *12* (11−12), 720−723.
(35) Almtiri, M.; Dowell, T. J.; Giri, H.; Wipf, D. O.; Scott, C. N. Electrochemically Stable Carbazole-Derived Polyaniline for Pseudocapacitors. *ACS Appl. Polym. Mater.* **2022**, *4* (5), 3088−3097.
(36) ASTM International. *G48-11 Standard Test Methods for Pitting and Crevice Corrosion Resistance of Stainless Steels and Related Alloys by Use of Ferric Chloride Solution*, DOI: 10.1520/G0048-11R20E01.
(37) Shao, W.; Jamal, R.; Xu, F.; Ubul, A.; Abdiryim, T. The Effect of a Small Amount of Water on the Structure and Electrochemical Properties of Solid-State Synthesized Polyaniline. *Materials* **2012**, *5*, 1811−1825.
(38) Shabani-Nooshabadi, M.; Ghoreishi, S. M.; Behpour, M. Direct Electrosynthesis of Polyaniline−Montmorrilonite Nanocomposite Coatings on Aluminum Alloy 3004 and Their Corrosion Protection Performance. *Corros. Sci.* **2011**, *53* (9), 3035−3042.
(39) Navarchian, A. H.; Joulazadeh, M.; Karimi, F. Investigation of Corrosion Protection Performance of Epoxy Coatings Modified by Polyaniline/Clay Nanocomposites on Steel Surfaces. *Prog. Org. Coat.* **2014**, *77* (2), 347−353.
(40) Shabani-Nooshabadi, M.; Ghoreishi, S. M.; Jafari, Y.; Kashanizadeh, N. Electrodeposition of Polyaniline-Montmorrilonite Nanocomposite Coatings on 316L Stainless Steel for Corrosion Prevention. *J. Polym. Res.* **2014**, *21*, 416.
(41) Babu, V. J.; Vempati, S.; Ramakrishna, S. Conducting Polyaniline-Electrical Charge Transportation. *Materials Sciences and Applications* **2013**, *4*, 1−10.
(42) Bui, T. T.; Tran, D. H.; Phan, H. M.; Dao, D. N.; Nguyen, Q. T.; Cu, S. T.; Nguyen, H. T. Synthesis and Optical Properties of Conjugated Copolymers Based on Phenoxazine and Fluorene for an Activated Layer in Polymeric Solar Cell Applications. *Science and Technology Development Journal* **2022**, DOI: 10.32508/stdj.v25i3.3970.
(43) Otteny, F.; Perner, V.; Wassy, D.; Kolek, M.; Bieker, P.; Winter, M.; Esser, B. Poly(Vinylphenoxazine) as Fast-Charging Cathode Material for Organic Batteries. *ACS Sustain Chem. Eng.* **2020**, *8* (1), 238−247.
(44) Rohom, A. B.; Londhe, P. U.; Mahapatra, S. K.; Kulkarni, S. K.; Chaure, N. B. Electropolymerization of Polyaniline Thin Films. *High Perform Polym.* **2014**, *26* (6), 641−646.
(45) Stejskal, J.; Trchová, M.; Bober, P.; Humpolíček, P.; Kašpárková, V.; Sapurina, I.; Shishov, M. A.; Varga, M. Conducting Polymers: Polyaniline. In *Encyclopedia of Polymer Science and Technology*; John Wiley & Sons, Inc.: 2015; pp 1−44.
(46) Trchová, M.; Morávková, Z.; Bláha, M.; Stejskal, J. Raman Spectroscopy of Polyaniline and Oligoaniline Thin Films. *Electrochim. Acta* **2014**, *122*, 28−38.
(47) Szatylowicz, H.; Jezuita, A.; Siodła, T.; Varaksin, K. S.; Domanski, M. A.; Ejsmont, K.; Krygowski, T. M. Toward the Physical Interpretation of Inductive and Resonance Substituent Effects and Reexamination Based on Quantum Chemical Modeling. *ACS Omega* **2017**, *2* (10), 7163−7171.
(48) Trivedi, D. J.; Barrow, B.; Schatz, G. C. Understanding the Chemical Contribution to the Enhancement Mechanism in SERS: Connection with Hammett Parameters. *J. Chem. Phys.* **2020**, DOI: 10.1063/5.0023359.
(49) Sharma, Y. R. *Elementary Organic Spectroscopy (Principles and Chemical Applications)*, 5th revised ed.; S. Chand & Company Pvt. Limited: New Delhi, 2007.
(50) Shakoor, A.; Rizvi, T. Z.; Nawaz, A. Raman Spectroscopy and AC Conductivity of Polyaniline Montmorillonite (PANI-MMT) Nanocomposites. *Journal of Materials Science: Materials in Electronics* **2011**, *22* (8), 1076−1080.
(51) Ghil, L.-J.; Youn, T.-Y.; Park, N.-R.; Rhee, H.-W. Proton Conductive Nano-Channel Membranes Based on Polyaniline with Phosphonic Acid Moieties for Low Relative Humidity. *J. Nanosci. Nanotechnol.* **2013**, *13* (12), 7912−7915.
(52) Iqbal, M.; Manzoor, S. Method of Enhancing Polyaniline Conductivity Using Different Oxidizing Agent as Dopant. *TechConnect Briefs* **2010**, *1*, 83−86.
(53) Caldona, E. B.; Smith, D. W.; Wipf, D. O. Protective Action of Semi-Fluorinated Perfluorocyclobutyl Polymer Coatings against Corrosion of Mild Steel. *J. Mater. Sci.* **2020**, *55* (4), 1796−1812.
(54) Beele, W.; Marijnissen, G.; van Lieshout, A. The Evolution of Thermal Barrier Coatings — Status and Upcoming Solutions for Today's Key Issues. *Surf. Coat. Technol.* **1999**, *120−121*, 61−67.
(55) Goswami, R. N.; Mourya, P.; Behera, B.; Khatri, O. P.; Ray, A. Graphene-Polyaniline Nanocomposite Based Coatings: Role of Convertible Forms of Polyaniline to Mitigate Steel Corrosion. *Appl. Surf. Sci.* **2022**, *599*, 153939.
(56) Hu, C.; Li, Y.; Zhang, N.; Ding, Y. Synthesis and Characterization of a Poly(o-Anisidine)−SiC Composite and Its Application for Corrosion Protection of Steel. *RSC Adv.* **2017**, *7* (19), 11732−11742.
(57) Bagherzadeh, M.; Mousavi, O.; Shams Ghahfarokhi, Z. Fabrication and Characterization of a Fe_3O_4/Polyvinylpyrrolidone (Fe_3O_4/PVP) Nanocomposite as a Coating for Carbon Steel in Saline Media. *New J. Chem.* **2020**, *44* (35), 15148−15156.
(58) Jiang, K.; Li, J.; Liu, J. Electrochemical Codeposition of Graphene Platelets and Nickel for Improved Corrosion Resistant Properties. *RSC Adv.* **2014**, *4* (68), 36245.
(59) Brunner, R.; Etsion, I.; Talke, F. E. A Simple Atomic Force Microscopy Calibration Method for Direct Measurement of Surface Energy on Nanostructured Surfaces Covered with Molecularly Thin Liquid Films. *Rev. Sci. Instrum.* **2009**, *80* (5), No. 055109.
(60) Chang, X.; Li, L.; Li, T.; Zhou, D.; Zhang, G. Accelerated Microrockets with a Biomimetic Hydrophobic Surface. *RSC Adv.* **2016**, *6* (90), 87213−87220.
(61) Zoppe, J. O.; Ataman, N. C.; Mocny, P.; Wang, J.; Moraes, J.; Klok, H. A. Surface-Initiated Controlled Radical Polymerization: State-of-the-Art, Opportunities, and Challenges in Surface and Interface Engineering with Polymer Brushes. *Chem. Rev.* **2017**, *117* (3), 1105−1318.
(62) Riul, A.; Dhanabalan, A.; Cotta, M.A.; Hermann, P.S.P.; Mattoso, L.H.C.; MacDiarmid, A.G.; Oliveria, O.N. AFM Studies of Composite 16-Mer Polyaniline Langmuir-Blodgett (LB) Films. *Synth. Met.* **1999**, *101* (1−3), 830−831.
(63) Ramphal, I. A.; Hagerman, M. E. Nanoscale Morphology, Tribology and Electrical Properties of Polyaniline/Graphene Oxide/LAPONITE® Composites Investigated Using Atomic Force Microscopy. *Nanoscale* **2019**, *11* (43), 20876−20883.

(64) Fosong, W.; Jinsong, T.; Lixiang, W.; Hongfang, Z.; Zhishen, M. Study on the Crystallinity of Polyaniline. *Molecular Crystals and Liquid Crystals Incorporating Nonlinear Optics* **1988**, *160* (1), 175−184.
(65) MacDiarmid, A. G.; Epstein, A. J. Polyanilines: A Novel Class of Conducting Polymers. *Faraday Discuss. Chem. Soc.* **1989**, *88* (0), 317−332.
(66) Ambalagi, S. M.; Devendrappa, M.; Nagaraja, S.; Sannakki, B. Dielectric Properties of PANI/CuO Nanocomposites. *IOP Conf Ser. Mater. Sci. Eng.* **2018**, *310* (1), No. 012081.
(67) Sanches, E. A.; Soares, J. C.; Mafud, A. C.; Fernandes, E. G. R.; Leite, F. L.; Mascarenhas, Y. P. Structural Characterization of Chloride Salt of Conducting Polyaniline Obtained by XRD, SAXD, SAXS and SEM. *J. Mol. Struct.* **2013**, *1036*, 121−126.
(68) Sokolova, M. P.; Smirnov, M. A.; Kasatkin, I. A.; Dmitriev, I. Y.; Saprykina, N. N.; Toikka, A. M.; Lahderanta, E.; Elyashevich, G. K. Interaction of Polyaniline with Surface of Carbon Steel. *Int. J. Polym. Sci.* **2017**, *2017*, 1−9.
(69) Chaudhari, H. K.; Kelkar, D. S. X-ray Diffraction Study of Doped Polyaniline. *J. Appl. Polym. Sci.* **1996**, *62* (1), 15−18.
(70) Sangaj, N. S.; Malshe, V. C. Permeability of Polymers in Protective Organic Coatings. *Prog. Org. Coat.* **2004**, *50* (1), 28−39.
(71) Gamry Instruments Inc. *Getting Started with Electrochemical Corrosion Measurement*, 2011. http://www.gamry.com/App_Notes/Understandin.
(72) Wessling, B. Passivation of Metals by Coating with Polyaniline: Corrosion Potential Shift and Morphological Changes. *Adv. Mater.* **1994**, *6* (3), 226−228.
(73) Nikravesh, B.; Ramezanzadeh, B.; Sarabi, A. A.; Kasiriha, S. M. Evaluation of the Corrosion Resistance of an Epoxy-Polyamide Coating Containing Different Ratios of Micaceous Iron Oxide/Al Pigments. *Corros. Sci.* **2011**, *53* (4), 1592−1603.
(74) Manoli, Z.; Pecko, D.; Van Assche, G.; Stiens, J.; Pourkazemi, A.; Terryn, H. Transport of Electrolyte in Organic Coatings on Metal. In *Paint and Coatings Industry*; IntechOpen: 2019.
(75) Dohare, S. Corrosion Protection and Modern Infrastructure. In *Introduction to Corrosion - Basics and Advances*; IntechOpen: 2023.
(76) Caldona, E. B.; de Leon, A. C. C.; Mangadlao, J. D.; Lim, K. J. A.; Pajarito, B. B.; Advincula, R. C. On the Enhanced Corrosion Resistance of Elastomer-Modified Polybenzoxazine/Graphene Oxide Nanocomposite Coatings. *React. Funct. Polym.* **2018**, *123*, 10−19.
(77) Hsu, C. H.; Mansfeld, F. Technical Note: Concerning the Conversion of the Constant Phase Element Parameter Y0 into a Capacitance. *CORROSION* **2001**, *57* (9), 747−748.
(78) Scribner Associates Inc. *ZView® 4.0 Operating Manual Impedance/Gain-Phase Graphing & Analysis Software*, rev. B.; 2021; Vol. *40*.
(79) Kanwal, S.; Akhter, Z.; Ali, N. Z.; Hussain, R.; Qamar, S. Corrosion Protection of Aluminum Alloy (AA2219-T6) Using Sulphonic Acid-Doped Conducting Polymer Coatings. *New J. Chem.* **2022**, *46* (30), 14557.
(80) Bagherzadeh, M.; Mousavi, O.; Ghahfarokhi, Z. S. Fabrication and Characterization of a Fe_3O_4/Polyvinylpyrrolidone (Fe_3O_4/PVP) Nanocomposite as a Coating for Carbon Steel in Saline Media. *New J. Chem.* **2020**, *44* (35), 15148−15156.
(81) Caldona, E. B.; Wipf, D. O.; Smith, D. W. Characterization of a Tetrafunctional Epoxy-Amine Coating for Corrosion Protection of Mild Steel. *Prog. Org. Coat.* **2021**, *151*, No. 106045.
(82) Rammelt, U.; Reinhard, G. Application of Electrochemical Impedance Spectroscopy (EIS) for Characterizing the Corrosion-Protective Performance of Organic Coatings on Metals. *Prog. Org. Coat.* **1992**, *21* (2−3), 205−226.
(83) Chen, H.; Yu, Z.; Cao, K.; Chen, L.; Pang, Y.; Xie, C.; Jiang, Y.; Zhu, L.; Wang, J. Preparation of a BTA−UIO−GO Nanocomposite to Endow Coating Systems with Active Inhibition and Passive Anticorrosion Performances. *New J. Chem.* **2021**, *45* (35), 16069−16082.
(84) Walter, G. W. A Review of Impedance Plot Methods Used for Corrosion Performance Analysis of Painted Metals. *Corros. Sci.* **1986**, *26* (9), 681−703.
(85) Wadhwani, P. M.; Panchal, V. K.; Shah, N. K. Investigation of Anti-Corrosive Properties of o-Anisidine-N-Salicylidene and Its Nanocomposite o-Anisidine-N-Salicylidene/NiONPs on Mild Steel in 2 N HCl. *RSC Adv.* **2016**, *6* (93), 90897−90915.
(86) Lu, H.; Zhang, S.; Li, W.; Cui, Y.; Yang, T. Synthesis of Graphene Oxide-Based Sulfonated Oligoanilines Coatings for Synergistically Enhanced Corrosion Protection in 3.5% NaCl Solution. *ACS Appl. Mater. Interfaces* **2017**, *9* (4), 4034−4043.
(87) Sun, M.; Ma, Z.; Li, A.; Zhu, G.; Zhang, Y. Anticorrosive Performance of Polyaniline/Waterborne Epoxy/Poly-(Methylhydrosiloxane) Composite Coatings. *Prog. Org. Coat.* **2020**, *139*, No. 105462.

https://doi.org/10.1021/acsapm.3c02347
ACS Appl. Polym. Mater. 2024, 6, 3060−3072